Engineering heme binding sites in monomeric rop

Engineering heme binding sites in monomeric rop.

Giovanna Di Nardo[1], Almerinda Di Venere[2], Giampiero Mei[2], Sheila J. Sadeghi[1], Jon R. Wilson[3] and Gianfranco Gilardi[1,3,✉].

[1] Department of Human and Animal Biology, University of Torino, via Accademia Albertina 13, 10123, Torino, Italy

[2] Department of Experimental Medicine and Biochemical Sciences, University of Rome 'Tor Vergata', Via Montpellier 1, 00133, Rome, Italy

[3] Division of Molecular Biosciences, Imperial College London, Biochemistry Building, South Kensington, London, SW7 2AY, UK

Corresponding author address: Department of Human and Animal Biology, via Accademia Albertina 13, 10123 Torino. Tel.: +390116704593; fax: +390116704643

Email address: gianfranco.gilardi@unito.it;

Abstract

Heme ligands were introduced in the hydrophobic core of an engineered monomeric ColE1 repressor of primer (rop-S55) in two different layers of the heptad repeat. Mutants rop-L63M/F121H (layer 1) and rop-L56H/L113H (layer 3) were found to bind heme with a K_D of 1.1±0.2 and 0.47±0.07 μM respectively. The unfolding of heme-bound and –free mutants, in the presence of guanidinium hydrochloride, was monitored by both circular dichroism and fluorescence spectroscopy. For the heme bound rop mutants, the total free energy change was 0.5 kcal/mol higher in the layer 3 mutant compared to that of layer 1. Heme binding also stabilized these mutants by increasing the ΔG_{obs}^{H2O} by 1.4 and 1.8 kcal/mol in rop-L63M/F121H and rop-L56H/L113H, respectively. The reduction potentials measured by spectroelectrochemical titrations were calculated to be -154±2 mV for rop-56H/113H and –87.5±1.2 mV for rop-L63M/F121H.

The mutant designed to bind heme in a more buried environment (layer 3) showed a tighter heme binding, a higher stability and a different reduction potential than the mutant designed to bind heme in layer 1.

Keywords: Heme, four helix bundle, rational design, rop, redox potential, synthetic biology.

Introduction.

One of the goals of protein engineering and synthetic biology is to use simple molecular scaffolds able to mimic more complex natural proteins. The first approach has been successfully used to introduce different co-factors including mononuclear iron centers and iron-sulfur clusters in existing proteins [1-3]. The second approach, the *de novo* design of proteins and metalloproteins adopting different folds, has extensively contributed to increase our knowledge about the problem of protein folding [4]. Furthermore, peptides designed to mimic the entire functionality of different enzymes can play an essential role to understand the properties governing the biological functions of proteins [5].

The four α-helix bundle is a robust motif found in many proteins in nature [6]. This fold is common to proteins with different functions ranging from electron transfer, metal storage and enzymatic activity [7]. For this reason, synthetic biology has been widely used for the de novo design of peptides predicted to have a four helix bundle structure [8-10] with the aim to obtain molecular scaffolds where to introduce new functions. These synthetic peptides not only have been demonstrated to incorporate biological and nonbiological cofactors [11-16], but also could mimic the functionality of entire enzymes such as heme oxygenases [17], thus giving the opportunity to better understand the behavior of more complex proteins. Furthermore, these constructs also have the potential to lead to new catalysts [18] and bioelectrochemical devices [19-20].

The cofactor heme has a relevant role in biology, as it is present in proteins with different functions including dioxygen storage and transport, electron transfer and oxygenation of different substrates. For this reason, synthetic biology has focused its attention to construct heme assemblies as models for their natural counterparts

[21]. An alternative method to produce heme proteins with a four-helix bundle structure is engineering an existing scaffold adopting this fold by rational design to create a heme binding site. Here we present the protein engineering of a RNA binding protein, the repressor of primer from *Escherichia coli* (rop).

Rop is the protein component involved in the control of ColE1 plasmid replication [22-23]. The native activity of rop is to bind to and stabilize the RNAI:RNAII replication initiation complex inhibiting subsequent plasmid replication. Rop is a small dimeric protein (14 kDa) that consists only of one basic secondary structural element, the α-helix. The tertiary fold of rop is a four-helix bundle slightly twisted to form a left-handed coiled-coil [24]. Rop has been the subject of extensive studies in protein folding also by site directed mutagenesis [25-27]. The effects of different mutations have been shown to not significantly affect the conformation of the protein especially if the hydrophobic core packing is retained [28-30].

The dimeric nature of rop does not allow the introduction of single point mutations in the four helix bundle scaffold, where each mutation would be replicated in the second monomer of the bundle. However, a modified version of a monomeric rop form (rop-S55) is available [31] in which all four helices are expressed as a single polypeptide chain linked by polyglycine loops of varying length. The construct rop-S55 containing two loops of five glycines was demonstrated to best retain the structural and functional properties of the natural dimeric protein [31]. For this reason, it was selected as scaffold to engineer a heme binding site by rational design. The introduction of redox functions into a simple molecular scaffold such as rop and the possibility to modulate the redox potential can provide a useful tool to i) understand the properties governing heme redox potential, ii) reproduce the properties of more complex enzymes, iii) construct biotechnological devices. Recently, another monomeric rop construct has been engineered to study the redox chemistry of a

unique tryptophan residue introduced into the molecular scaffold of the protein [32] giving further evidence on the possibility to use this protein as a model for enzymology studies.

In a preliminary work, we demonstrated how this simple natural protein lacking physiological prosthetic groups has been adapted to bind heme on the basis of its structural resemblance to natural redox proteins such as cytochromes [33]. The mutant rop-L56H/L113H demonstrated also to be electrochemically active with a reduction potential of –154 mV measured by spectroelectrochemistry [33]. Here, we designed a new mutant with a different heme coordination and position into the rop scaffold in order to investigate if it is possible to tune the reduction potential of the new heme binding proteins making them useful for different applications We explored the secondary structure, the stability and unfolding pathway of the engineered heme binding proteins before and after heme insertion and we compared these properties with those found for the starting monomeric rop constructs. The heme binding of the two mutants were then studied as well as the electrochemical behaviour.

Materials and Methods

Materials

Chemicals were obtained from Sigma-Aldrich Company Limited (Dorset, UK) unless otherwise stated. Enzymes for molecular biology and chromatography supports were obtained from Amersham Biotech UK Limited (Buckinghamshire, UK).

Design of rop heme binding mutant

Models of the structure of monomeric rop-S55 and derivatives were created using the InsightII 95.0 package (MSI) on an SGI Indigo Impact 10000. The rop wild-type NMR structure (pdb ID: 1rpr, model 2) was used as the starting template. Within the HOMOLOGY module of InsightII the sequence of monomeric rop was aligned with the appropriate regions of the dimeric structure so that helices 1/2/3/4 of the monomeric model were derived from 1/1'/2'/2 of the NMR structure. The lowest energy conformers of 5 glycine loops linking the 1/2 (1/1') and 3/4 (2/2') helices generated by the software were selected. The model was refined by energy minimization using the DISCOVER 3.0 module within InsightII using the CVFF forcefield. Models of rop mutants with and without heme were derived from this monomeric structure using the ESFF forcefield.

The monomeric construct, rop-S55, in which helices 1 and 2 and helices 3 and 4 are connected via loops of five glycine residues was the starting point for the rational design strategy [31].

Site directed mutagenesis was performed either by the "QuikChange" method (Stratagene, Europe) in which a circular plasmid is amplified using two complementary oligonucleotides containing the desired mutation. DNA manipulations were carried out in *E. coli* DH5α or *E. coli* XL1-Blue (Stratagene, Europe). The rop

gene was amplified by PCR using Pfu Turbo DNA polymerase and flanking primers and mutations were confirmed by sequencing of the PCR product (DNA Sequencing Service, Department of Biological Sciences, Imperial College, London).

Overexpression, purification and characterization of rop variants

The strategy for overexpression and purification of rop variants was developed based on the published procedure for the wild type protein [34]. Rop mutants in the pMR103 plasmid were expressed in *E. coli* BL21 (λDE3) by induction from the T7 promoter by addition of isopropyl-β-D-thiogalatctopyranoside (1 mM) (Melford Laboratories). A crude extract was prepared by cell lysis (Sonication; Sonics Vibracell with stepped microtip, Sonics and Materials Inc., USA) followed by centrifugation (Sorval RC5C Plus, rotor SS34, 18 000 rpm, 20 minutes) at 4 ºC. Ion exchange chromatography was performed using DEAE Fast Flow Sepharose. The buffer system was 10 mM Tris pH 7.8, 1mM EDTA, 1 mM DTT. A linear gradient of 200 to 400 mM NaCl was used to elute the protein. Size exclusion chromatography was performed initially using Superdex 75 (GE Healthcare). Purification was monitored by SDS polyacrylamide gel electrophoresis (Phast system, Amersham Biotech).

Hemin chloride was prepared in dimethyl formamide and then diluted in 10 mM sodium phosphate buffer, pH 8.0, 100 mM NaCl which had been flushed with oxygen free nitrogen and used immediately. For heme titrations a protein solution (2.5 μM for rop-L63M/F121H and 1 μM for rop-L56H/L113H) was titrated with hemin chloride (ranging from 0 to 7.5 μM for rop-L63M/F121H with first additions of 0.25 μM and from 0 to 7 μM for rop-L56H/L113H with first additions of 0.1 μM). After

each addition the solution was allowed to equilibrate for 10 minutes at 20 ºC and a spectrum collected (Hewlett Packard 8543 UV-visible diode array spectrophotometer). Titration of hemin chloride in buffer were also performed to collect free heme spectra that were subtracted to the corresponding obtained in presence of the protein. The increase in absorbance at 413 nm was plotted versus the heme concentration and fitted by Sigma Plot Software 8.0 to the following 1:1 ligand binding equation:

$$y = A\ x\ /\ (K_D + x) \qquad (1)$$

where A is the difference absorbance at 413 nm and K_D the dissociation constant.

For electrochemical and structural studies bulk preparations of heme bound rop were made by incubation of protein with a five-fold excess of hemin chloride overnight at 4 ºC. Unbound heme was removed by chromatography with DEAE matrix. The resulting heme bound protein was concentrated and buffer exchanged by ultrafiltation (Amicon, Millipore, UK).

Circular dichroism measurements

CD spectra were recorded on a Jasco-710 spectropolarimeter, at 20 °C, using a 0.1 cm and 1.0 cm quartz cuvette in the UV and visible region, respectively.

Steady-state fluorescence spectra upon excitation at 280 or 293 nm, were collected using a photon counting spectrofluorometer (ISS, Model K2, USA). The optical absorption measurements were carried out with a Perkin Elmer Lambda 18 spectrophotometer.

Equilibrium Unfolding Measurements

Protein denaturation was obtained incubating the protein with different amounts of guanidinium hydrochloride (GdHCl) for 12 h at 4°C. Refolding of fully unfolded samples was achieved by diluting the denaturant concentration with buffer. The analysis of the fluorescence and circular dichroism unfolding transitions were performed according to a single pathway following the scheme:

$$N \underset{}{\overset{K}{<\!\!-\!\!>}} U$$

where N and U represent the native and unfolded protein fractions respectively. The experimental data, Y, have been fitted using the linear combination as shown in the following equation:

$$Y = Y_N f_N + Y_U f_U \quad (2)$$

where Y_N and Y_U are free parameters that correspond to the spectroscopic properties of each state; f_N and f_U are the protein fractions in the native and unfolded state for each denaturant concentration ($f_N + f_U = 1$).

The equilibrium constant K_U and the free energy change ΔG_{obs}^{u} were derived from the equations:

$$K_U = f_U / (1 - f_U) = f_U / f_N \quad (3)$$

$$\Delta G_{obs}^{U} = - RT \ln K_U \quad (4)$$

According to linear extrapolation method [35], the unfolding free energy is correlated to the denaturant concentration by the equation:

$$\Delta G_{obs}^{U} = \Delta G_{obs}^{H2O} - m\,[GuHCl] \quad (5)$$

where m is the molar cosolvent term, ΔG_{obs}^{H2O} is the the free energy extrapolated to 0 M [GuHCl] and [GuHCl] is the denaturant concentration.

The analysis of the rop mutants fluorescence unfolding transitions required a double step denaturation pathway following the scheme:

$$N \overset{K_1}{<\!\!-\!\!>} I \overset{K_2}{<\!\!-\!\!>} U$$

In this scheme, N, I and U represent the native, intermediate and unfolded protein species, respectively, while K_1 and K_2 are the two equilibrium constants.

The experimental data have been interpolated according to the equation:

$$Y = Y_N f_N + Y_I f_I + Y_U f_U \quad (6)$$

where

$f_N + f_I + f_U = 1$

$f_N = 1/(1+K_1+K_1K_2)$

$f_I = K_1/(1+K_1+K_1K_2)$

$f_U = K_1K_2/(1+ K_1+ K_1K_2)$

Electrochemistry of heme bound rop mutant

Cyclic voltammetry was performed in a modified Hagen cell on a bare glassy-carbon electrode activated with nitric acid [36]. The cell contained a saturated calomel reference electrode and platinum counter electrode and was continuously flushed with oxygen-free nitrogen. The protein concentration was 30 μM in a de-aerated buffer of 10 mM sodium phosphate, pH 8.0 + 100 mM NaCl. The potentiostat was an Autolab

PGSTAT 10 (Eco Chemie BV, Holland) and cyclic voltammetry was performed over a range –0.2 to +0.2 Volts controlled by GPES3 Software.

Spectroelectrochemical titrations were performed with sodium dithionite as the reductant in a gas tight cell housed in a quartz cuvette (Hellma Limited, UK) with a platinum-mesh working electrode and Ag/AgCl as reference electrode continuously flushed with oxygen-free nitrogen. The mediators (phenazine methosulphate (5 μM), duraquinone (5 μM), 2-hydroxy 1,4 napthoquinone (5 μM), benzyl viologen (2 μM), indigocarmine (0.5 μM), resorufin (0.5 μM) were added to cover the full potential range of the titration. Additions of sodium dithionite (0.5 μl of a 10 mM solution) were added and spectra were collected after the potential stabilized. The fraction of reduced protein was estimated at each potential by following the shift in Soret peak (413 to 426 nm) and the data fitted to the Nernst equation for a single electron:

$$E = E_m + (RT/nF) \ln ([ox] / [red]) \quad (7)$$

where E is the solution reduction potential at equilibrium, E_m is the midpoint potential, R the gas constant, T the absolute temperature, n is the number of electrons F the Faraday constant and [ox] and [red] the concentrations of the oxidized and reduced species respectively.

Results and Discussion

Design of rop heme binding mutant

The monomeric rop-S55 scaffold [31] was used as a template to introduce the heme binding sites. To this end, a model was generated by homology modeling starting from the known structure of dimeric rop [37]. As shown in figure 1, the model of monomeric rop retains the general features of the wild type dimeric structure. The analysis of the model revealed the presence of four solvent exposed histidine residues (H76, H78, H107, H109, see figure 1B). In order to avoid aspecific binding of heme, these histidines were mutated (H76A, H78W, H107A, H109W, see table I) giving rise to the mutant rop-JW2. As wild type rop does not contain tryptophan residues, the mutations into tryptophan resulted in the insertion of a fluorescent marker useful for unfolding studies.

TABLE I.

The choice of suitable sites for the introduction of heme binding residues was based on the analysis of the layers forming the hydrophobic core of monomeric rop. These were numbered according to the nomenclature of Munson et al., [38] and they are shown in figure 1c. Cross sections of each layer shows the presence of four aminoacids, two in position “a” (small side chains) and two in “d” (large side chains) [38]. Positions “d” of layers 1 and 3 were chosen for the introduction of the heme ligands leading to mutants rop-L63M/F121H (layer 1, figure 1d) and rop-L56H/L113H (layer 3, figure 1e).

FIGURE 1.

Overexpression, purification and characterization of mutants

Both rop-L63M/F121H and rop-L56H/L113H mutants were successfully expressed and purified by ionic exchange chromatography and gel filtration. One single band at a molecular weight of 14.6 kDa was obtained (figure 2a) and yields of 2 mg of pure protein per liter of culture were obtained. The gel filtration profile also indicated that the mutants are monomeric.

FIGURE 2

The heme binding was obtained by mixing the protein with a five-fold excess of heme. After removal of the excess heme, the UV-visible spectrum was recorded and the presence of an absorbance maximum at 413 nm was observed (figure 2B). After reduction of rop-L63M/F121H with sodium dithionite, the visible spectrum showed a shift of the λ_{max} from 413 nm to 426 nm and the α and β bands were detected at 535 and 559 nm respectively (figure 2B). For rop-L56H/L113H, a shift of the λ_{max} from 413 nm to 424 nm was reported after reduction and the bands were detected at 531 and 559 nm [33]. These spectra are characteristic of heme containing six-coordinate low-spin Fe(II) [39]. Furthermore, the Soret bands of rop mutants are typical of *b*-type cytochromes [21,40].

Figure 3a shows the spectra obtained from the titration of rop-L63M/F121H with heme. The increase in absorbance at 413 nm indicates the incorporation of the prosthetic group. The titration was performed also for rop-L56H/L113H and also in this case an increase in the absorbance at 413 nm was observed (data not shown). The values obtained at 413 nm for the two mutants were then plotted versus the heme concentration and the data fitted to a 1:1 ligand binding equation. Figures 3b and 3c show the curves obtained for rop-L63M/F121H and rop-L56H/L113H respectively. The dissociation constants resulted to be 1.1 ± 0.2 μM and 0.47 ± 0.07 μM for rop-

L63M/F121H (layer 1) and rop-L56H/L113H (layer 3) respectively. These data indicate a two folds tighter binding of heme on the mutant designed to bind the prosthetic group in a more hydrophobic environment. In fact, in rop-L56H/L113H heme is in contact with at least five hydrophobic residues (Leu54, Ile71, Met12, Phe15, Cys72) whereas in rop-L63M/F121H only Leu118 and Met1 are in the near surrounding of heme, as predicted by the models. These K_D values are in the same range of those measured for the synthetic helix bundle where dissociation constants of 0.8-5 μM were reported [41].

FIGURE 3.

The far-UV circular dichroism (CD) spectra of rop-S55, rop-JW2 and heme bound rop are reported in figure 4. While the rop-S55 construct showed the same secondary structure content of wild type rop [42], the insertion of two tryptophan residues (JW2) produced a decrease in the CD signal, probably due to helix distorsion. An even larger change was observed in the presence of the additional mutations in rop-L63M/F121H and rop-L56H/L113H in the absence of heme, indicating that the insertion of the histidine and methionine residues caused a local disruption of the hydrophobic core deemed necessary to allow heme binding. Nevertheless, the presence of two maxima at 208 and 222 nm indicates a high helical content. The CD spectra of the heme-bound rop-L63M/F121H and rop-L56H/L113H resulted to be similar to that of the heme-free mutants, suggesting that the heme insertion does not cause significant changes in the protein secondary structure.

FIGURE 4.

Equilibrium unfolding measurements

Equilibrium unfolding experiments have been carried out by measuring the change of both the intrinsic fluorescence and the circular dichroism signals. The data points shown in figure 5a and 5b represent the overall average of three measurements obtained by fluorescence spectroscopy plus three by circular dichroism. The unfolding of rop-S55 and rop-JW2 (figure 5a) resulted to be very similar. For both proteins the unfolding process is fitted by a single transition curve with equal free energy changes (8.7 kcal/mol, table II). The introduction of tryptophan residues does not affect the protein stability even if some conformational changes occur, as observed by CD measurements.

TABLE II

In the case of heme-free rop-L63M/F121H and rop-L56H/L113H mutants, a two-step transition model is necessary to fit the data and the resulting total free energy change resulted 5.6±1.1 kcal/mol and 5.7±0.7 kcal/mol for rop-L63M/F121H and rop-L56H/L113H, respectively. The introduction of heme binding ligands resulted in a loss of stability of the scaffold, as expected by mutating the residues forming the hydrophobic core of the protein.

Also for heme-bound rop-L63M/F121H and rop-L56H/L113H, a two-step transition model is necessary to adequately fit the data (figure 5b), though in this case a total free energy change of 7.0±1.0 kcal/mol and 7.5±1.1 kcal/mol respectively was calculated (table II). As the unfolding followed by far-UV circular dichroism overlaps that obtained from tryptophan fluorescence emission (figure 5b), the intermediate detected for the engineered rop proteins cannot correspond to a molten globule state.

The changes of rop-L63M/F121H and rop-L56H/L113H absorption spectra in the visible region as a function of guanidinium hydrochloride (GdHCl) concentration were also measured. As shown in the inset of figure 5b, most of the signal at 413 nm is already lost at 3 M GdHCl thus indicating that the loosening of the heme group

takes place during the first transition during unfolding. Both heme-bound mutants display a higher ΔG_{obs}^{H2O} value with respect to the heme-free samples. This enhanced stability essentially concerns the first step of the unfolding transition, as shown by the larger $\Delta G_{obs}^{H2O}{}_1$ and m_1 values reported in Table II. The addition of the heme group has effects on the protein stability increasing the $\Delta G_{obs}^{H2O}{}_1$ value with respect to the heme unbound proteins (table II) and giving a stability to the mutants more similar to the initial rop-S55 construct. Furthermore, the parameter m is related to the steepness of the unfolding transition curve and is a measure of the hydrophobicity of the protein core [43]. The increase of m_1 value (table II), known to be linearly proportional to the increase of the solvent accessible area during unfolding [44], demonstrates that the heme prostethic group was incorporated in the protein core of rop mutants.

The difference in $\Delta G_{obs}^{H2O}{}_1$ values between the two heme-bound mutants demonstrates that heme insertion in a more buried position in rop-L56H/L113H (layer 3) gives more stability to the scaffold.

FIGURE 5

Figure 5c shows the tryptophan fluorescence emission spectra of heme-bound and heme-free rop-L63M/F121H. The emission maximum resulted to be shifted from 325 nm for the heme-bound rop-L63M/F121H to 343 nm for the heme-free form. This demonstrates that the incorporation of the heme macrocycle induces a change in the tertiary structure of the protein. Similar results were also found for rop-L56H/L113H where a shift from 338 to 347 nm is observed upon heme incorporation.

Analysis of the data show that both mutants behave in the same way. Figure 5d proposes a model for the unfolding pathway consistent with circular dichroism and fluorescence data. The insertion of heme into the mutants involves changes in the tertiary structure, as suggested by fluorescence spectroscopy. Both the heme-bound and -free forms denature into an intermediate where secondary and tertiary structures

are partially lost as detected by equilibrium unfolding experiments. In the case of the heme-bound forms, the heme is lost during the first transition. A stabilising role of the heme was found for both mutants as shown by ΔG_{obs}^{H2O} values measured in the heme-bound forms. A second transition going from the intermediate to the unfolded states is common to the heme-bound and -free mutants and shows similar ΔG_{obs}^{H2O} values.

Electrochemistry of heme binding mutant

Cyclic voltammetry of heme-bound rop-L63M/F121H was performed on glassy carbon electrode in the absence of mediators. The midpoint potential (E_{mid}) calculated with respect to the normal hydrogen electrode resulted to be -100 ± 14 mV. The oxidative and reductive peak currents were found to have a linear relationship with respect to the scan rate. This indicates that the mutant is immobilized on the surface of the electrode. These results are consistent with those obtained for rop-L56H/L113H where the midpoint potential calculated by cyclic voltammetry is –134 ± 13 mV and the protein is adsorbed onto the electrode [33].

Spectroelectrochemistry was also used to determine the reduction potential and the results for rop-L63M/F121H and rop-L56H/L113H mutants are shown in figure 6. Fitting to the Nernst equation led to reduction potentials of -87.5 ± 1.2 mV for rop-L63M/F121H and -154 ± 2 mV for rop-L56H/L113H. In the latter mutant also a smaller component at 17 ± 9 mV was observed as discussed in Wilson et al., 2003.

FIGURE 6

The reduction potential determined for the rop variants resulted similar to those reported for synthetic helix bundle heme protein designs [45-46] and within the range of natural cytochromes [47] suggesting a successful incorporation and ligation of the heme.

The difference in reduction potentials observed in rop mutants can be mainly caused by the different axial ligands present in the two mutants. In fact, it is well known that Met-His ligated hemes have a more positive reduction potential than His-His coordinated hemes in both synthetic and natural protein [48-49]. In particular, in the Heme Protein Database [49], it was found that in the main α-helical proteins the reduction potential can range from –412 mV to +450 mV. By considering the heme coordination motifs, the His-His heme coordinated proteins have reduction potentials ranging from –412 to +380 mV, whereas for the Met-His coordinated molecules the range varies from –60 to +450 mV [49]. While the reduction potential of the mutant rop-L56H/L113H lies in the range of His-His coordinated heme proteins, the mutant rop-L63M/F121H with a Met-His heme coordination shows a reduction potential slightly more negative than the range reported in the Heme Protein Database. However, other parameters including heme exposure to the solvent [50], distortion of porphyrin prosthetic groups [51], hydrophobicity and alteration of local electrostatic [52] can play important roles in controlling the reduction potential. In the case of the mutant rop-L63M/F121H, the heme binds in layer 1 and its solvent accessibity, calculated by using the Mark Gerstein's Software [53], resulted 31 $Å^2$ whereas for the mutant rop-L56H/L113H it resultes 27 $Å^2$. This parameter could justify the lower reduction potential found in rop-L63M/F121H in comparison to the others Met-His heme proteins.

Conclusions.

In conclusion, this work supports the possibility to introduce new functions into existing molecular scaffolds by protein engineering. The mutant rop-L56H/L113H, designed to have a His-His heme binding site in a more buried environment in the core of the protein (layer 3) resulted to have a tighter heme binding, a higher total

stability and a more negative reduction potential when compared to the mutant rop-L63M/F121H, where the Met-His heme binding site was designed in the more solvent exposed layer 1. The opportunity to tune the heme binding properties, the stability and the reduction potential of rop according to the heme ligands and position offers a solid model for studying different natural heme proteins and to match a required biotechnological application.

Acknowledgements

The monomeric rop construct, pMR103-S55, was kindly provided by Prof. Lynne Regan, Department of Molecular Biophysics and Biochemistry, Yale University, New Haven, USA. We thank MIUR project (PRIN) and Piedmont Regional Government (CIPE) for financial support.

Tables

Table I. Rop mutants obtained using the monomeric rop-S55 as template. Four histidines residues were removed in rop-JW2 to avoid aspecific heme binding. One histidine and one methionine (rop-L63M/F121H) and two histidines (rop-L56H/L113H) were introduced in rop-JW2 to allow heme binding in specific positions of rop scaffold.

Construct	Mutations on rop-S55 [27]
rop-JW2	H76A, H78W, H107A, H109W
rop-L63M/F121H	H76A, H78W, H107A, H109W, L63M, F121H
rop-L56H/L113H	H76A, H78W, H107A, H109W, L56H, L113H

Table II. Thermodynamic parameters characterizing the chemical unfolding process of the rop mutants.

Protein	**$\Delta G_{obs}^{H2O}1$ (kcal/mol)**	**m1 (kcal/mol)**	**$\Delta G_{obs}^{H2O}2$ (kcal/mol)**	**m2 (kcal/mol)**	**Total ΔG_{obs}^{H2O} (kcal/mol)**
rop-S55	8.7±0.7	2.4±0.3			8.7±0.7
rop-JW2	8.7±0.8	1.9±0.5			8.7±0.8
rop-L63M/F121H	1.8±0.5	0.9±0.2	3.8±0.6	0.8±0.3	5.6±1.1
rop-L63M/F121H + heme	3.1±0.5	2.9±0.2	3.9±0.5	1.1±0.3	7.0±1.0
rop-L56H/L113H	1.7±0.1	0.9±0.1	4.0±0.6	0.8±0.2	5.7±0.7
rop-L56H/L113H + heme	3.5±0.6	3.0±0.9	4.0±0.5	1.0±0.2	7.5±1.1

Figures

Fig. 1. Ribbon representation of (a) native dimeric rop (pdb ID: 1rpr); (b) model of rop-S55 with histdine residues shown in stick representation (purple); (c) protein backbone of rop (blue) with hydrophobic core side chains (orange) at different layers (1 to 8); (d) side and top views of rop-L63M/F121H with bound heme (red); (e) side and top views of rop-L56H/L113H with bound heme (red).

Fig. 2. a) SDS-PAGE gel of purified rop-L63M/F121H corresponding to the band at 14.6 kDa (lane 1 purified rop-L63M/F121H; lane 2 molecular weight markers); b) visible spectra of rop-L63M/F121H (1 μM) in the oxidized (solid line) and reduced (dashed line) forms.

Fig. 3. a) Absorption spectra of rop-L63M/F121H with added increasing concentrations of heme. b) Binding curve obtained by plotting the absorbance at 413 nm versus heme concentration for mutant rop-L63M/F121H and c) for rop-L56H/L113H. In both cases the corresponding absorbance of free heme was subtracted.

Fig. 4. Circular dichroism spectra of rop-S55 (large dashes), rop-JW2 (short dashes), rop-L63M/F121H (dotted line) and rop-L56H/L113H (solid line).

Fig. 5. Panel a: dependence of the unfolded protein fraction on GdHCl concentration for rop-S55 (black circles) and rop-JW2 (black squares). Panel b: dependence of the unfolded protein fraction for rop- L56H/L113H (black squares) and rop-L63M/F121H (white squares). Inset: the absorption of rop-L56H/L113H plus

heme is reported as a function of GdHCl. Panel c: tryptophan fluorescence emission spectra of rop-L63M/F121H with (solid line) and without (dotted line) heme. Panel d: model for the unfolding pathway of rop mutants with and without heme consistent with circular dichroism and fluorescence data.

Fig. 6. Spectroelectrochemical titrations for rop-L63M/F121H (black circles) and rop-L56H/L113H (open circles).

References

1. Farinas E, Regan L. 1998 Protein Sci. 7:1939–1946
2. Benson DE, Wisz M, Liu W, Hellinga HW (1998) Biochemistry 37:7070-7076
3. Benson DE, Wisz MS, Hellinga HW (2000) Proc Natl Acad Sci U S A 97:6292-7
4. DeGrado WF, Summa CM, Pavone V, Nastri F, Lombardi A (1999) Ann Rev Biochem, 68:779-819
5. Cowley AB, Kennedy ML, Silchenko S, Lukat-Rodgers GS, Rodgers KR, Benson DR (2006) Inorg Chem 45:9985-10001
6. Harris N, Presnell S, Cohen F (1994) J Mol Biol 236:1356-1368
7. Kamtekar S, Hecht MH (1995) FASEB J 9:1013-1022
8. Grove A, Mutter M, Rivier JE, Montal M (1993) J Am Chem Soc 115:5919-5924
9. Choma CT, Lear JD, Nelson MJ, Dutton PL, Robertson DE, DeGrado WF (1994) J Am Chem Soc 116:856-865
10. Betz S, Liebman P, DeGrado WF (1997) Biochemistry 36:2450-2458
11. Robertson D, Farid R, Moser C, Urbauer J, Mulholland S, Pidikiti R, Lear J, Wand A, DeGrado WF, Dutton P (1994) Nature 368:425-431
12. Gibney B, Mulholland S, Rabanal F, Dutton P (1996) Proc Natl Acad Sci U S A 93:15041-15046
13. Gibney BR, Johansson JS, Rabanal F, Skalicky JJ, Wand AJ, Dutton PL (1997) Biochemistry 36:2798-2806
14. Sharp R, Diers J, Bocian D, Dutton P (1998) J Am Chem Soc 120:7103-7104
15. Cochran F, Wu S, Wang W, Nanda V, Saven J, Therien M, DeGrado WF (2005) J Am Chem Soc 127:1346-1347
16. Bender G, Lehmann A, Zou H, Cheng H, Fry H, Engel D, Therien M, Blasie J, Roder H, Saven J, DeGrado WF (2007) J Am Chem Soc 129:10732-10740
17. Monien B, Drepper F, Sommerhalter M, Lubitz W, Haehnel W (2007) J Mol Biol 371:739-753
18. Rau H, DeJonge N, Haehnel W (1998) Proc Natl Acad Sci U S A 95:11526-11531
19. Topoglidis E, Discher BM, Moser CC, Dutton PL, Durrant JR (2003)

Chembiochem 4:1332-1339

20. Willner I, Heleg-Shabtai V, Katz E, Rau H, Haehnel W (1999) J Am Chem Soc 121:6455-6468
21. Lombardi, F. Nastri, V. Pavone, (2001) Chem Rev 101:3165-3189
22. Helmer-Citterich M, Anceschi M, Banner D, Cesareni G (1988) EMBO J 7:557-566
23. Cesareni G, Helmer-Citterich M, Castagnoli L (1991) Trends Genet 7:230-235
24. Banner D, Kokkinidis M, Tsernoglou D (1987) J Mol Biol 196:657-675
25. Hoffmann D, Knapp EW (1997) J Phys Chem B 101:6734-6740
26. Kokkinidis M, Vlassi M, Papanikolaou Y, Kotsifaki D, Kingswell A, Tsernoglou D, Hinz HJ (1993) Proteins 16:214-216
27. Steif C, Hinz H, Cesareni G (1995) Proteins 23:83-96
28. Ceruso M, Grottesi A, Di Nola A (1999) Proteins 36:436-446
29. Predki P, Agrawal V, Brünger A, Regan L (1996) Nat Struct Biol 3:54-58
30. Vlassi M, Cesareni G, Kokkinidis M (1999) J Mol Biol 285:817-827
31. Predki P, Regan L (1995) Biochemistry 34:9834-9839
32. Westerlund K, Moran SD, Privett HK, Hay S, Jarvet J, Gibney BR, Tommos C (2008) Protein Eng Des Sel 21:645-52
33. W ilson J, Caruana D, Gilardi G (2003) Chem Commun (Camb):356-357
34. Munson M, Predki P, Regan L (1994) Gene 144:59-62
35. Schellman J (1987) Biopolymers 26:549-559
36. Hagen W (1989) Eur J Biochem 182:523-530
37. Eberle W, Pastore A, Sander C, Rösch P (1991) J Biomol NMR 1:71-82
38. Munson M, O'Brien R, Sturtevant J, Regan L (1994) Protein Sci 3:2015-2022
39. Adar F (1978), In: Dolphin D (ed) The Porphyrins. Electronic absorption spectra of hemes and heme proteins. Academic Press Inc., New York, pp. 167-209.
40. Yu L, Xu J, Haley P, Yu C (1987) J Biol Chem 262:1137-1143
41. Shifman J, Gibney B, Sharp R, Dutton P (2000) Biochemistry 39:14813-14821
42. Peters K, Hinz H, Cesareni G (1997) Biol Chem 378:1141-1152

43. Pace NC, Shirley BA, Thomson JA (1990) In: Creghton TF (ed.) Protein Structure: A Practical Approach. IRL Press, Oxford, pp. 311-330.

44. Myers JK, Pace CN, Scholtz JM (1995) Protein Sci 4:2138-2148

45. Gibney B, Huang S, Skalicky J, Fuentes E, Wand A, Dutton P (2001) Biochemistry 40:10550-10561

46. Xu ZJ, Farid RS (2001) Protein Sci 10:236-249

47. Chapman SK, Daff S, Munro AW (1997) Metal Sites in Proteins and Models, pp. 39-70

48. Reedy CJ, Gibney BR Chem Rev (2004) 104:617-49

49. Reedy CJ, Elvekrog MM, Gibney BR (2008) Nucleic Acids Res 36: D307-13

50. Stellwagen E (1978) Nature 275:73-74

51. Shelnutt JA, Song XZ, Ma JG, Jia SL, Jentzen W, Medforth CJ (1998) Chem Soc Reviews 27:31-41

52. Gunner MR, Alexov E, Torres E, Lipovaca S (1997) J Biol Inorg Chem 2:126-134

53. Gerstein M (1992) Acta Crystallographica Section A 48:271-276

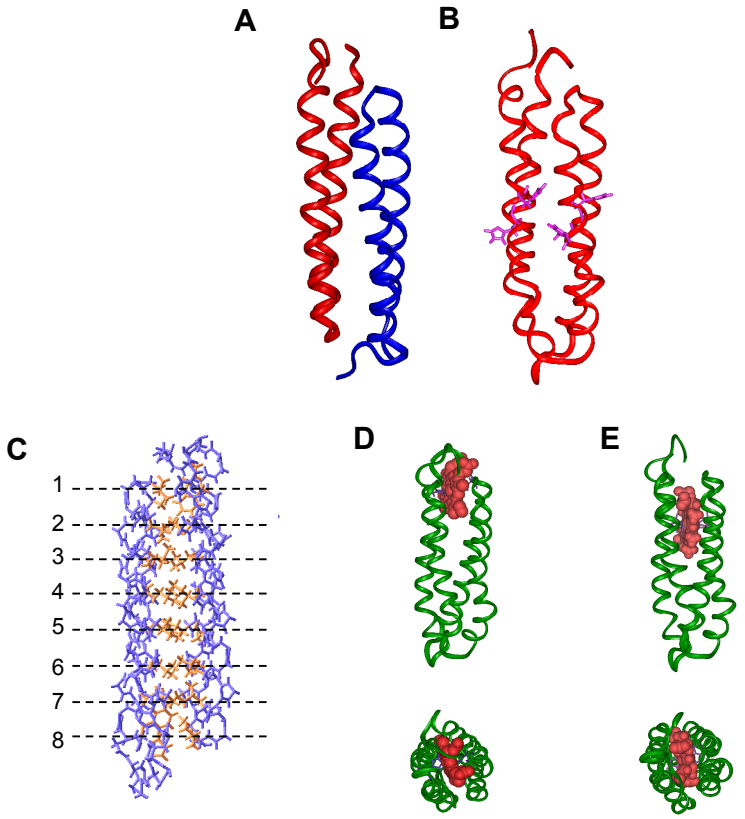

FIGURE 1 Di Nardo et al.

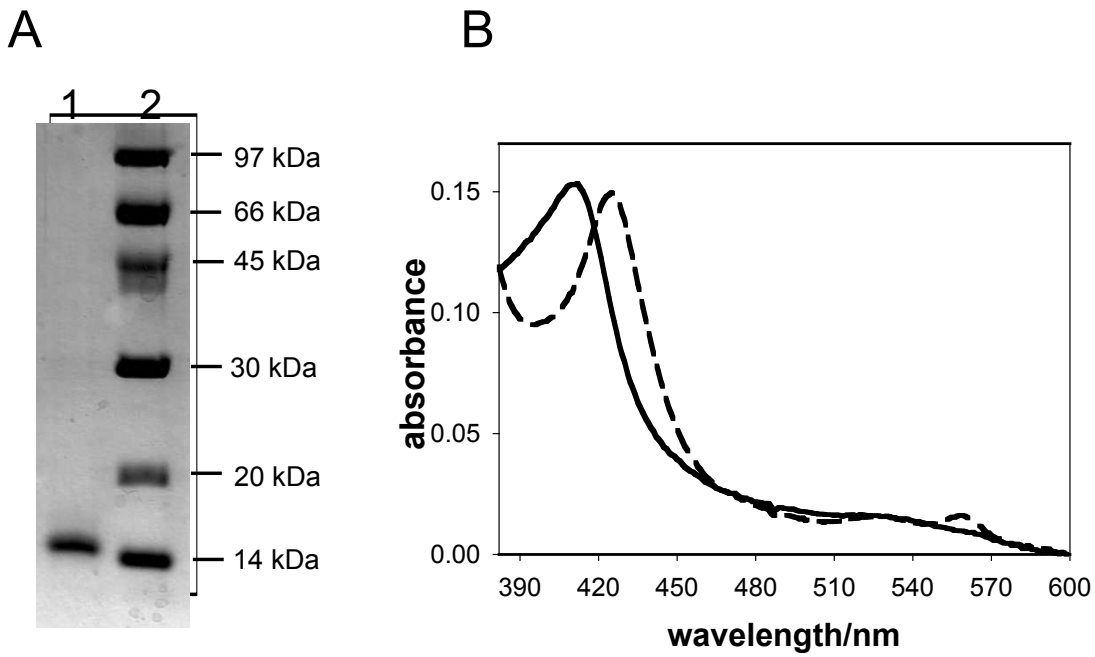

FIGURE 2 Di Nardo et al.

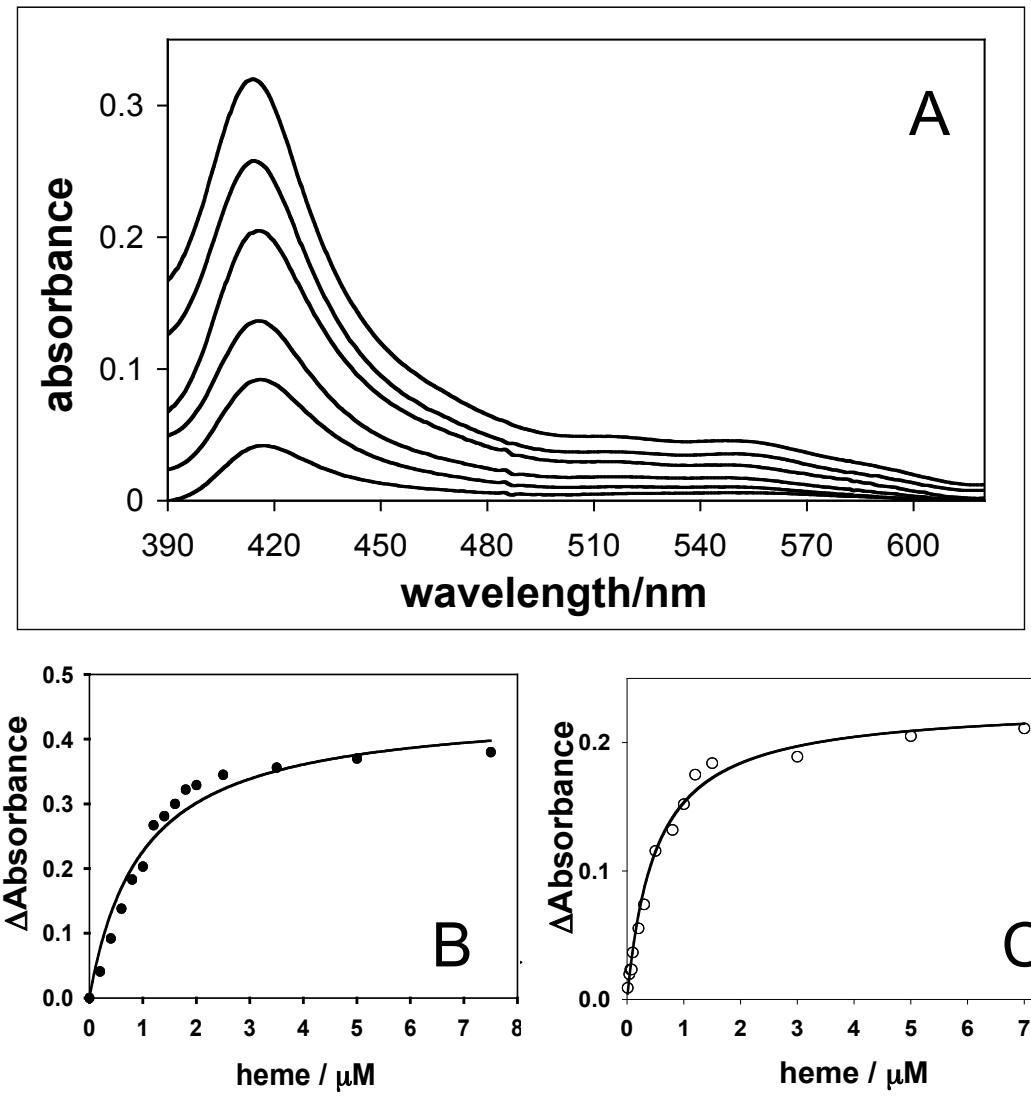

FIGURE 3 Di Nardo et al.

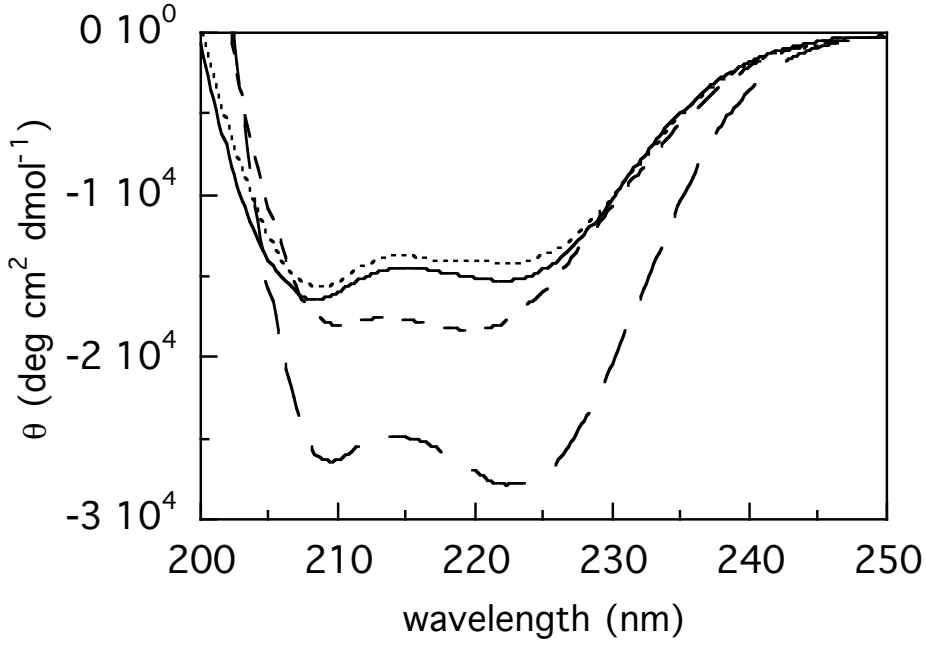

FIGURE 4 Di Nardo et al.

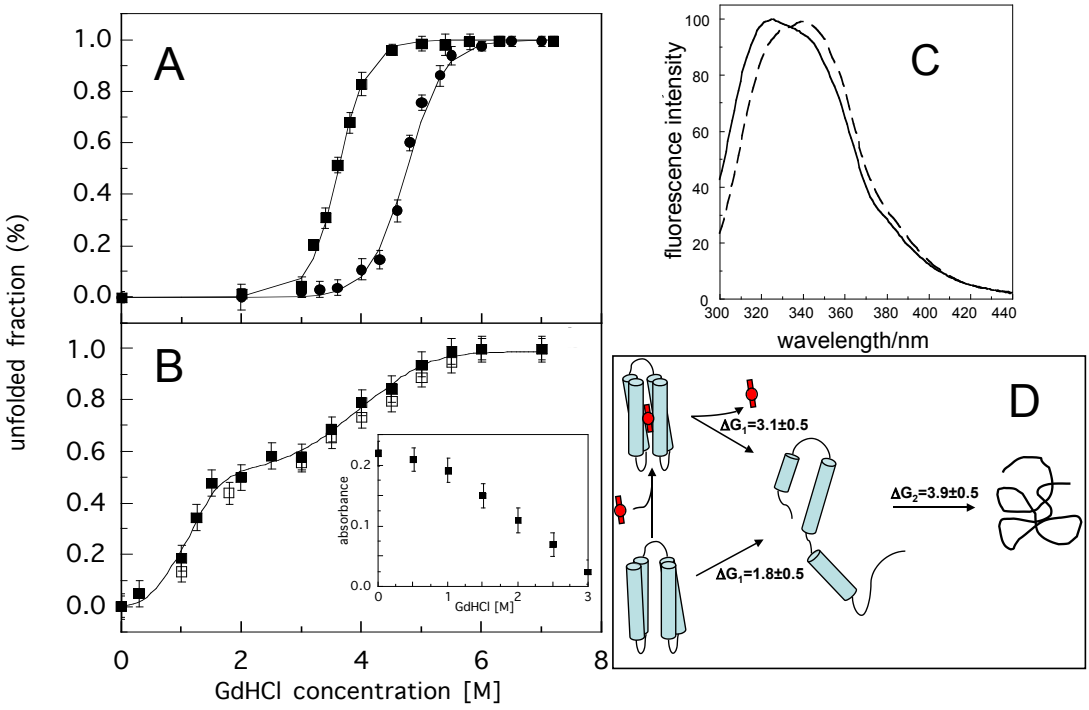

FIGURE 5 Di Nardo et al.

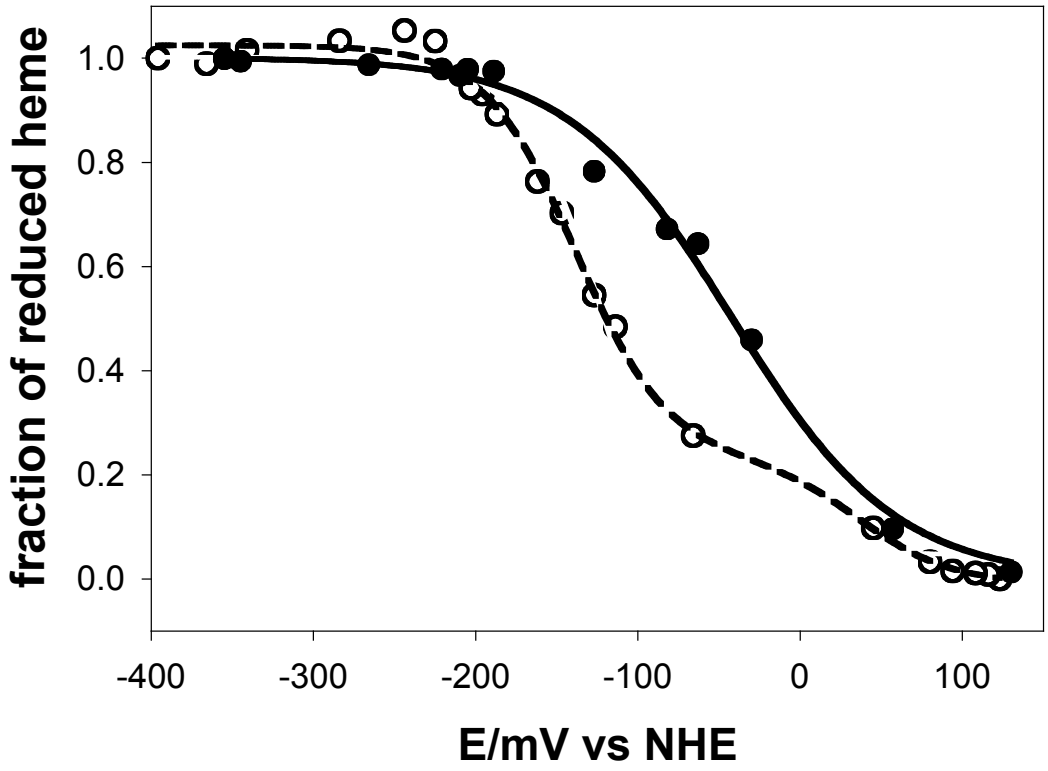

FIGURE 6 Di Nardo et al.